Hindawi
Journal of Chemistry
Volume 2021, Article ID 5841066, 11 pages
https://doi.org/10.1155/2021/5841066

Research Article

Mesoporous $LaFeO_3$: Synergistic Effect of Adsorption and Visible Light Photo-Fenton Processes for Phenol Removal from Refinery Wastewater

Thi To Nga Phan,[1] **Hong Lien Nguyen**,[1] **Van Tuyen Le**,[1] **Chi Nhan Phan**,[2] **and Thanh Huyen Pham**[1]

[1]*Department of Organic and Petrochemical Technology, School of Chemical Engineering, Hanoi University of Science and Technology, Hanoi, Vietnam*
[2]*Center for Chemical Accident Response and Safety, Vietnam Chemicals Agency, Ministry of Industry and Trade of the Socialist Republic of Vietnam, Hanoi, Vietnam*

Correspondence should be addressed to Thi To Nga Phan; nga.phanthito@hust.edu.vn

Received 28 April 2021; Revised 10 May 2021; Accepted 25 May 2021; Published 3 June 2021

Academic Editor: Ibrahim H. Alsohaimi

Mesoporous $LaFeO_3$ as a visible light-driven photocatalyst was prepared by a nanocasting method using mesoporous silica (SBA-15) as a hard template. The as-prepared $LaFeO_3$ photocatalyst was characterized by X-ray diffraction (XRD), scanning electron microscopy (SEM), transmission electron microscopy (TEM), N_2 adsorption-desorption, X-ray photoelectron spectroscopy (XPS), and optical absorption spectra. The characterization studies and experimental results showed that $LaFeO_3$ with porous structure caused by the removal of SBA-15 hard template could enhance the specific surface area of the resulting photocatalyst, which improves the phenol adsorption ability of the photocatalyst and in turn enhances its photo-Fenton catalytic activity. The photo-Fenton catalytic activity of the photocatalyst was investigated by photo-Fenton degradation of aqueous phenol under visible light irradiation. The effects of catalyst dosage, H_2O_2 concentration, and solution pH on the photo-Fenton catalytic degradation of phenol using mesoporous $LaFeO_3$ were studied and optimized. Under the optimal conditions of 20 mg L^{-1} phenol, 1.0 g L^{-1} catalyst, and 10 mM H_2O_2 at pH = 5, the photo-Fenton degradation of phenol (93.47%) was achieved in 180 min under visible light irradiation. Furthermore, our results proved the stability and reusability of mesoporous $LaFeO_3$ and revealed its catalytic mechanism for the photo-Fenton degradation of phenol.

1. Introduction

Untreated wastewater released from many industries such as paper making; petrochemical, textile, and flavouring agents; and petroleum industry contains high phenol concentrations. Phenol is considered as a hazardous and lethal pollutant that could be one of the main sources of harm to our ecosystem and human health [1]. The US Environmental Protection Agency (USEPA) has listed phenol as a foremost contaminant due to its poor degradability and high toxicity and suggested a permissible limit of phenol deposition less than 0.5 ppm in wastewater [2, 3]. In this frame, strategies for wastewater remediation of phenol are extremely essential.

Various technologies have been recently developed for wastewater treatment [4–6]. Wang et al. investigated the use of $LaCu_{0.5}Co_{0.5}O_3$ perovskite intercalated montmorillonite and g-C_3N_4 nanocomposites on microwave-induced H_2O_2 catalytic degradation of bisphenol A [7]. This technique shows several advantages such as fast reaction rate, rapid selective heating, efficient degradation of a variety of organic contaminants, and no secondary pollution [7, 8]. Meanwhile, adsorption is also considered as a promising method for wastewater treatment due to its convenience, cost-

effectiveness, simple operation, and environmental reasons [6]. In order to treat phenol-containing wastewater, several methods have been employed such as biological, stripping, and adsorption processes; however, these methods did not allow completely mineralizing phenol due to its recalcitrant nature [9]. Therefore, high-efficiency technologies such as Advanced Oxidative Processes (AOPs) should be applied. AOPs are based on the generation of hydroxyl radicals, very strong oxidizing species, that are able to chemically degrading a wide range of organic pollutants into innocuous products and in turn reduce the levels of pollution in wastewater [10, 11]. AOPs consist of photocatalysis, UV, UV/O_3, UV/H_2O_2, O_3/H_2O_2, Fenton, photo-Fenton processes, and catalytic wet peroxide oxidation [12–14]. Among these AOPs, the photo-Fenton process has been found to be the most promising method in terms of the process efficiency based on organic contaminants removal and operation cost [15]. Recently, the utilization of solar energy appears to be an effective strategy for addressing environmental concerns and energy crises [16–18]. Considering the use of solar power, semiconductor photocatalysts, especially iron-containing photocatalysts with narrow band gap energy belonging to the perovskite family, have been developed to decompose organic pollutants under visible light irradiation [19–22].

As one of the commonly iron-contained perovskite oxides, $LaFeO_3$ is considered as a promising visible light-driven photocatalyst for the photo-Fenton degradation of organic pollutants [19, 23–26]. During the photo-Fenton reaction, the organic pollutants could be oxidized by the attack of hydroxyl radicals; it is, therefore, necessary to improve the contact area between the active sites on to photocatalyst surface and organic compounds. However, the practical applications of the perovskite materials are limited due to the fact that they owe large particle size and small specific surface area causing by the traditional preparation methods such as sol-gel process, coprecipitation, and solution combustion [27]. Therefore, many strategies have been developed to overcome this shortcoming by improving their surface area via several novel methods, including the modified sol-gel process [28], nanocasting strategy [29, 30], polystyrene added sol-gel [31], and biotemplate method [32]. Of these methods, the nanocasting pathway using a hard template has attracted recent research interest due to its unique features such as controlled morphology and texture and highly crystallized walls of target materials [33]. Kaliaguine and coworkers prepared a series of perovskite oxides with the formula $LaBO_3$ (B = Mn, Co, Fe) via the nanocasting method [30]. The resulting samples exhibited extremely high specific surface areas, which are in a range of 110–155 m^2 g^{-1}. Wang et al. synthesized mesoporous $LaCoO_3$ by a similar method to that of Kaliaguine's group [29]. The results showed that $LaCoO_3$ possessed a specific surface area of 96.7 m^2 g^{-1} which is much higher than that synthesized by the conventional citrate method. Interestingly, all the hard templates used in these studies are mesoporous silica. The enhancement of the specific surface area of materials is believed to play an important role in the transportation of organic pollutants to active sites on its surface, improvement of its adsorption capability, and catalytic degradation [34].

In this work, the mesoporous $LaFeO_3$ photocatalyst was prepared by a nanocasting method using mesoporous silica (SBA-15) as a hard template. After filling the $LaFeO_3$ precursor into mesoporous channels of SBA-15, the hard template was then leached by NaOH solution. The adsorption capability and photo-Fenton-like catalytic activity for phenol removal over mesoporous $LaFeO_3$ were systematically studied. The effects of different operational parameters were investigated to determine the highest phenol removal efficiency. To the best of our knowledge, no such work has been previously published.

2. Materials and Methods

2.1. Materials. Tetraethyl orthosilicate ($Si(OC_2H_5)_4$; 99%), pluronic P123 ($EO_{20}PO_{70}O_{20}$; $M_n \sim 5800$), lanthanum nitrate hexahydrate ($La(NO_3)_3.6H_2O$; 99.9%), iron nitrate nonahydrate ($Fe(NO_3)_3.9H_2O$; ≥98%), citric acid ($C_6H_8O_7.H_2O$; 99.9%), hydrogen peroxide (H_2O_2; 30 wt%), and phenol (C_6H_5OH; 99.5%) were purchased from Sigma-Aldrich. Other chemicals were obtained from our lab in Vietnam. All chemicals were used without additional purifications.

2.2. Photocatalyst Preparation

2.2.1. Synthesis of Hard Template SBA-15. The hard template (HT) was synthesized according to Zhao's research [35]. 3.5 g of P123 was firstly dissolved in 100 mL of 1.5 M HCl under vigorous stirring for 2 h. Subsequently, 8.5 g of TEOS was added to the above solution and the resulting solution was kept at room temperature for 15 h. After that, the final mixture was allowed to stir at 40°C for 24 h before transferring into a Teflon-lined autoclave for hydrothermal treatment at 90°C for 48 h. The obtained solid product was filtered and rinsed with DI water several times before being dried at 80°C in an oven overnight. The obtained SBA-15 powder was then calcined in the air from 25°C to 550°C for 6 h (heating rate of 1°C/min^{-1}).

2.2.2. Synthesis of Mesoporous $LaFeO_3$ (LFO-RHT). Mesoporous $LaFeO_3$ (LFO-RHT) was prepared by the nanocasting method. Typically, 1.241 g of $La(NO_3)_3.6H_2O$, 1.158 g of $Fe(NO_3)_3.9H_2O$, and 1.205 g of citric acid were added to 5 mL of DI water. The mixture was kept on stirring for 3 h at ambient temperature, after which 1 g of SBA-15 was added. This resulting solution was continuously stirred at 70°C for 3 h and then dried at 350°C in an oven for 12 h. The SBA-15 filled with LFO was obtained by calcination at 700°C for 6 h. To remove the SBA-15 hard template, the obtained powder was treated with NaOH 8 M solution at 80°C for 4 h. Finally, the powders were centrifuged, washed with deionized water several times, and then dried in the oven at 60°C overnight. The resulting sample was named LFO-RHT. For comparison, pure LFO was synthesized using the similar method above in the absence of SBA-15 and used

to compare with LFO-RHT in the photo-Fenton degradation of phenol.

2.3. Characterization of Materials. Powder X-ray diffraction (XRD) patterns of samples were collected on a Bruker D8 diffractometer (Bruker, USA) using CuKα as radiation. The data was collected in 2θ range 10–80° with a step size of 0.02°/s. Scanning electron microscopy (SEM) (Zeiss 1555 VP-FESEM, Germany) was used to examine the surface morphology of the sample. Transmission electron microscopy (TEM) was taken using HRTEM (H7500, HITACHI). X-ray photoelectron spectroscopy of the target sample was taken on an X-ray photoelectron spectrometer (XPS, Kratos AXIS Ultra DLD, UK). The nitrogen adsorption-desorption isotherms were measured at 77 K on MICROMERITICS 2020 analyzer (Micromeritics, USA). The surface areas of samples were determined by using the Brunauer–Emmett–Teller (BET) method. The optical absorption spectra were recorded from 200 to 800 nm on a PerkinElmer LAMBDA 750 UV/Vis/NIR spectrophotometer (PerkinElmer, USA).

2.4. Removal of Phenol over LFO-RHT. The photo-Fenton experiments were carried out in a 250 ml cylindrical glass reactor with 70 mm in diameter and 115 mm in length. To avoid heating inside the reactor, it was surrounded by a circulating water jacket. A Xenon arc lamp of 300 W (LOT-Quantum Design) was used with a 400 nm cut-off filter as the source of visible light irradiation. 100 ml phenol solution of 20 mg L^{-1} and LFO-RHT was prepared and added to the reactor. Prior to light irradiation, the suspension was magnetically stirred in the dark for 60 min to reach an adsorption-desorption equilibrium of phenol onto LFO-RHT. To perform the photo-Fenton-like reaction, 1 ml H_2O_2 aqueous solution was dispersed in the suspension and the lamp was turned on to commence the photo-Fenton reaction. A small amount of sample was extracted from the reactor every 15 min and centrifuged for measurement.

2.5. Analytical Method. Perkin Elmer Lambda 750 UV–Vis spectrophotometer was used as the analytical technique for confirming the concentration of phenol. The maximum absorbance wavelength of phenol was found at 272 nm. The photo-Fenton degradation efficiency (%) was evaluated as follows:

$$\text{degradation efficiency } (\%) = \left(1 - \frac{C_t}{C_1}\right) \times 100\%, \quad (1)$$

where C_1 and C_t are the phenol concentrations before the photo-Fenton degradation and after time t in the photo-Fenton reaction, respectively.

To understand the degradation kinetics of phenol, the pseudo-first-order model was used (Mahmoodi et al., 2006):

$$-\ln \frac{C_t}{C_1} = kt. \quad (2)$$

where C_t is the concentration of phenol after time t in the photo-Fenton reaction and k is the pseudo-first-order rate constant. The rate constant (k) was calculated from the slope of the plot of ln (C_t/C_1) versus time.

The total removal rate of phenol was calculated as

$$\text{Removal rate } (\%) = \left(1 - \frac{C_i}{C_0}\right) \times 100\%, \quad (3)$$

where C_0 is the phenol concentrations before starting adsorption and C_i is the phenol concentrations after time i during the adsorption-photo-Fenton degradation process.

2.6. Reusability Experiments. The reusability of the photocatalyst was performed by repeating the photo-Fenton degradation tests (four times) under the above similar reaction conditions.

3. Results and Discussion

3.1. Material Characterization. The wide-angle XRD patterns of LFO and LFO-RHT are shown in Figure 1(a) and the XRD patterns of SBA-15 and LFO-RHT at low angles are included in Figure 1(b). As can be seen clearly from the low angle XRD, SBA-15 showed a strong characteristic peak at $2\theta = 1°$ and two small diffraction peaks at $2\theta = 1.7$ and 1.9° that could be assignable to the (100), (110), and (200) plane of SBA-15 [36], confirming the success in the synthesis of hard template SBA-15. As expected, in the wide-angle XRD pattern of the LFO-RHT, several characteristic peaks appeared at 2θ of 22.6, 32.2, 39.6, 46.3, 52.0, 57.4, 67.4, 72.0, and 76.7°, which are identical to those in the XRD pattern of our synthesized LFO [37]. The sample LFO-RHT exhibited the characteristic diffraction peaks indexable to the orthorhombic structure of LFO (JCPDS no. 37-1493). Note that the small-angle XRD of LFO-RHT (the inset in Figure 1(b)) showed the diffraction peak that could be indexed to the lattice plane (100) of SBA-15. Although the peak intensity was much lower than that of SBA-15, it still confirmed the existence of the SBA-15 hard template which was not able to be completely removed by NaOH solution [29, 30].

The general morphologies of LFO and LFO-RHT before and after alkali leaching are presented in Figures 2(a)–2(c). LFO is composed of nanosized particles, aggregating into large clumps, as shown in Figure 2(a). As can be seen in Figure 2(b), prior to removing SBA-15 by NaOH solution, the LFO-RHT sample showed agglomerated irregular shaped particles with the diameter in a range of 40–150 nm whilst the morphology of LFO-RHT after the removal of SBA-15 exhibited porous architecture with mesopores diameters in the range of 10–200 nm that were interconnected together (Figure 2(c)). This implies that the filling in the porous structure of SBA-15 and then removing of the SBA-15 hard template have significant influences on the morphology of LFO-RHT. TEM image in Figure 2(d) confirmed the porous structure of LFO-RHT after removing the SBA-15 hard template.

The nitrogen adsorption-desorption isotherms and BJH pore size distribution curves of LFO-RHT are shown in Figure 3. The N_2 adsorption-desorption isotherm curves of LFO-RHT showed a type IV isotherm with H_2-hysteresis

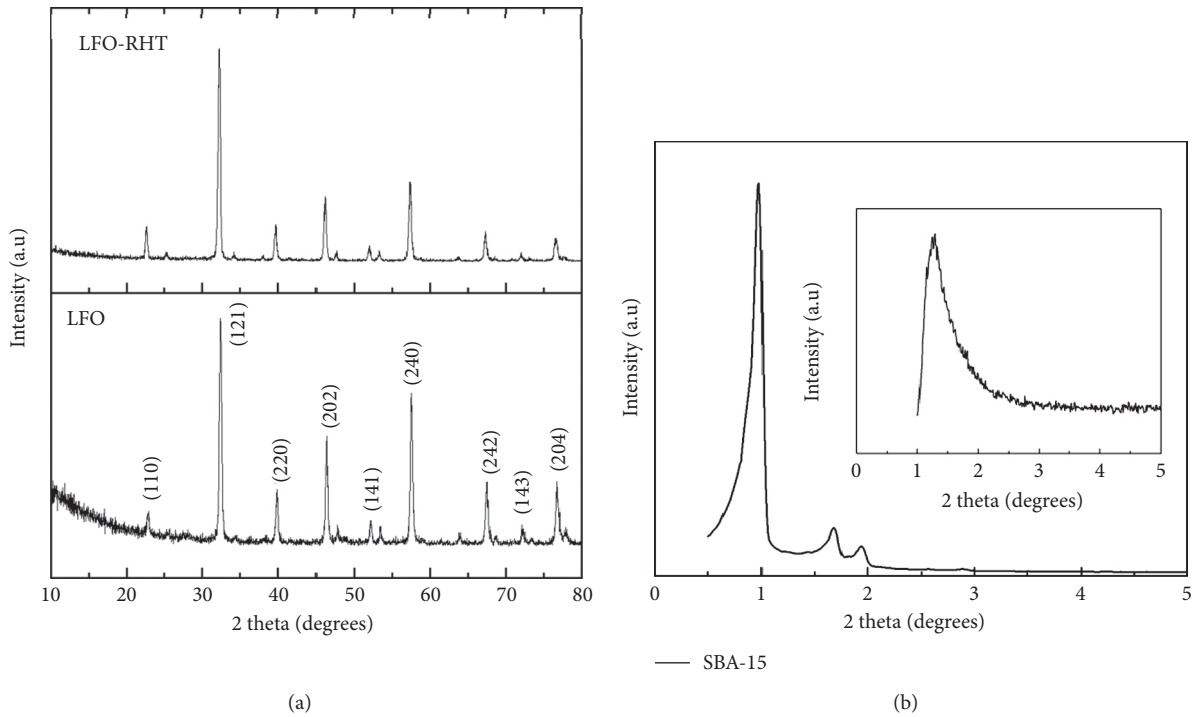

Figure 1: (a) XRD patterns of LFO and LFO-RHT and (b) XRD pattern of SBA-15 at low angles (the inset: XRD patterns of LFO-RHT at low angles).

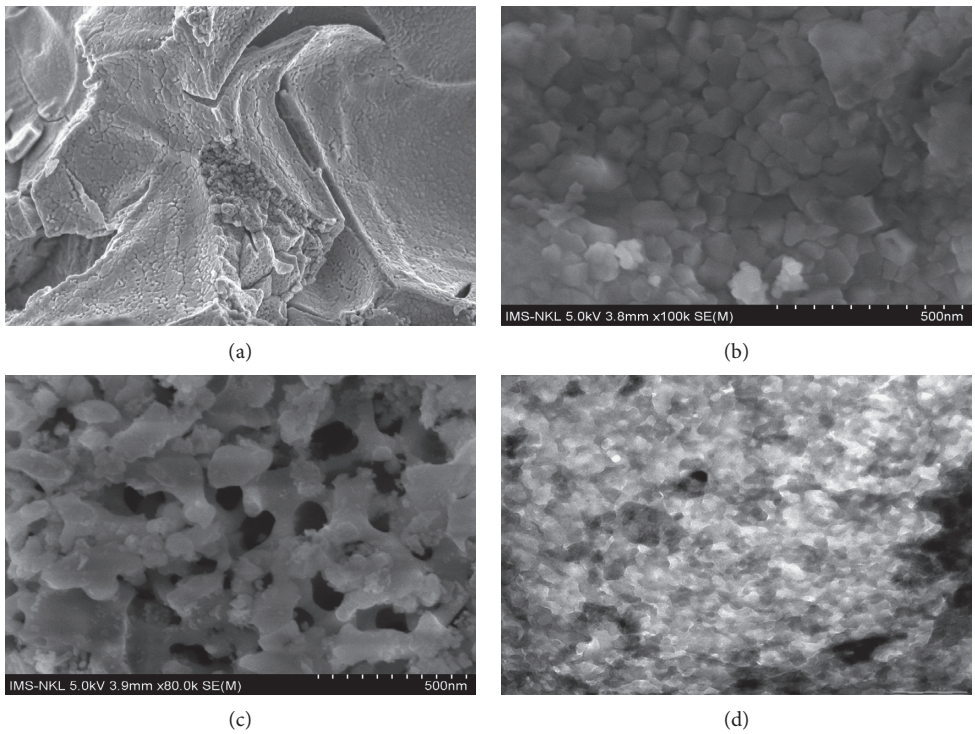

Figure 2: SEM images of (a) LFO, (b-c) LFO-RHT before and after removing SBA-15 hard template; and (d) TEM images of LFO-RHT.

loop appearing in a relative pressure range of 0.4–1 [5], as depicted in Figure 3(a). This suggests the characteristic of the presence of mesopores in the LFO-RHT sample due to the removal of the hard template [33, 38]. It can be seen from Figure 3(b) that the LFO-RHT exhibited a broad pore size distribution with bimodal mesopores peaks at around 10 and 50 nm. The LFO-RHT samples possessed larger specific areas ($48.75\,m^2\ g^{-1}$) than the pure LFO sample ($8.06\,m^2\ g^{-1}$),

which was advantageous to provide more active sites for the adsorption and photo-Fenton degradation to take place and enhancing removal efficiency. In literature, Zhang et al. also reported the improved specific surface area of mesoporous $LaCoO_3$ preparing by the nanocasting method [29]. The textual properties of LFO-RHT are listed in Table 1.

To estimate the surface elemental composition and the valence states of principle elements in LFO-RHT, the XPS spectra of LFO-RHT were investigated. The results presented in Figure 4 revealed the presence of La, Fe, and O elements in the LFO-RHT sample. The La 3d spectrum was examined to evidence the valence of La in Figure 4(a). The main two peaks at around 834 and 850 eV were assigned to La $3d_{5/2}$ and La $3d_{3/2}$ of La^{3+} [24]. The appearance of two peaks at around 710 and 728 eV, consigning to the binding energies of $Fe2p_{3/2}$ and Fe $2p_{1/2}$ on the Fe2p XPS spectrum (Figure 4(b)), implies the existence of Fe^{3+} oxidation state [39]. Figure 4(c) depicts the O 1s spectrum with two major peaks centering at around 528 and 531 eV, which were attributed to the crystal lattice oxygen and chemisorbed oxygen species, respectively [23].

As is well known that the performances of photocatalysts are highly related to their optical properties [40], Figure 5 illustrates the UV-Vis absorption spectra and the corresponding band gap energy of LFO-RHT. The band gap value was calculated from the interception of a linear fit to the low-energy side in a plot of $[F(R)hv]^2$ versus hv based on the following equation [41]:

$$F(R) = \frac{(1-R)^2}{2R}, \tag{4}$$

where hv is the energy of the incident photon, $F(R)$ is the Kubelka Munk function, and R is reflectance.

It can be seen from Figure 5(a) that the absorption spectra of LFO-RHT showed strong absorption in the visible region (400–800 nm). In Figure 5(b), the band gap value of LFO-RHT was estimated to be 1.96 eV, implying its suitability for photodegradation of pollutants under visible light irradiation.

3.2. Photo-Fenton Catalytic Degradation of Phenol

3.2.1. Effect of Different Catalysts on the Removal of Phenol. The removal of phenol using LFO and LFO-RHT via adsorption and photo-Fenton degradation under visible light irradiation is presented in Figure 6(a). It can be found that the tests utilizing no catalyst showed phenol removal of 0% in the absence of H_2O_2 and 8.9% in the presence of H_2O_2. Meanwhile, the LFO sample removed 1.4% and 73.50% of phenol via dark adsorption and photo-Fenton degradation, respectively. Interestingly, the adsorption capacity and photo-Fenton catalytic performance of LFO-RHT were considerably improved in comparison with LFO. The phenol removal rate after 60 min adsorption and 180 min visible light exposure were 12.7% and 94.7%, respectively. This could be attributed to the enhancement of dark adsorption thanks to the mesoporous structure of LFO-RHT, which then facilitates the subsequent photo-Fenton degradation of phenol under visible light irradiation [42]. The dynamics analysis of the phenol photo-Fenton degradation was studied as well. To better understand the reaction kinetic of phenol degradation, the pseudo-first-order model was applied. As can be seen from the pseudo-first-order kinetics in Figure 6(b), LFO-RHT exhibited higher apparent rate constants which are 0.0192 and 2.1 times over that of LFO, implying its faster photo-Fenton degradation rate and better photo-Fenton catalytic activity. Obviously, the modification of the morphology and texture can enhance the photo-Fenton catalytic activity of pure catalyst of $LaFeO_3$.

Figure 6(c) shows the time-dependent absorbance spectrum of LFO-RHT in the phenol photo-Fenton degradation. When irradiation time increased, the absorption maximum of phenol at $\lambda = 272$ nm gradually decreased. There was a slight change in the absorption maximum for LFO-RHT after 120 min exposure to visible light.

3.2.2. Effect of Parameters on the Photo-Fenton Degradation of Phenol. The effects of catalyst dosage, H_2O_2 concentration, and initial pH solution on the photo-Fenton degradation of phenol versus irradiation time are presented in Figures 7(a)–7(c). Figure 7(a) indicates that the photo-Fenton degradation efficiency increased with an increase of catalyst dosage. It could be ascribed to the increase of the number of active sites on the photocatalyst surface and subsequently the formation of hydroxyl radicals. A similar trend has been reported in Wei's study [43]. The highest degradation rate of 94.7% (corresponding total removal rate of 95.37%) was obtained at catalyst loading of 1 g L^{-1} and then decreased. A possible reason is that, as the catalyst dosage increases, the reaction suspension becomes more turbidity, leading to reducing the penetration of visible light into it and in turn decreasing the generation of OH radicals [42]. The observed pseudo-first-order reaction rate constant k for phenol degradation at the catalyst dosages of 0.5, 0.8, 1.0, and 1.2 g L^{-1} were 0.0146, 0.0179, 0.0192, and 0.0082 min^{-1}, respectively. Yu et al. reported similar observations for the photo-Fenton degradation of phenol by using Fe_3O_4-GO nanocomposite [44]. Therefore, 1 g L^{-1} was identified as the optimal catalyst dosage for the photo-Fenton degradation of phenol using LFO-RHT in our work.

In the heterogeneous photo-Fenton system, the influence of H_2O_2 concentration is important for the degradation of phenol because the amount of formed OH radicals depends on the H_2O_2 concentration [45]. In general, H_2O_2 concentration has effects on the photo-Fenton reaction via the following two opposing cases: (i) as the H_2O_2 concentration was increased, the phenol removal rate was enhanced due to the increasing of OH radicals which are available for a phenol attack; (ii) at higher concentration of H_2O_2, the excess amount H_2O_2 in the reaction solution could react with OH radicals to produce less reactive hydroperoxyl radicals (HO_2) (the following equation) and in turn lower photo-Fenton degradation efficiency [46]:

$$OH + H_2O_2 \longrightarrow HO_2 + H_2O \tag{5}$$

As can be seen in Figure 7(b), a maximum total removal rate of 95.37% was achieved with an optimal value of H_2O_2

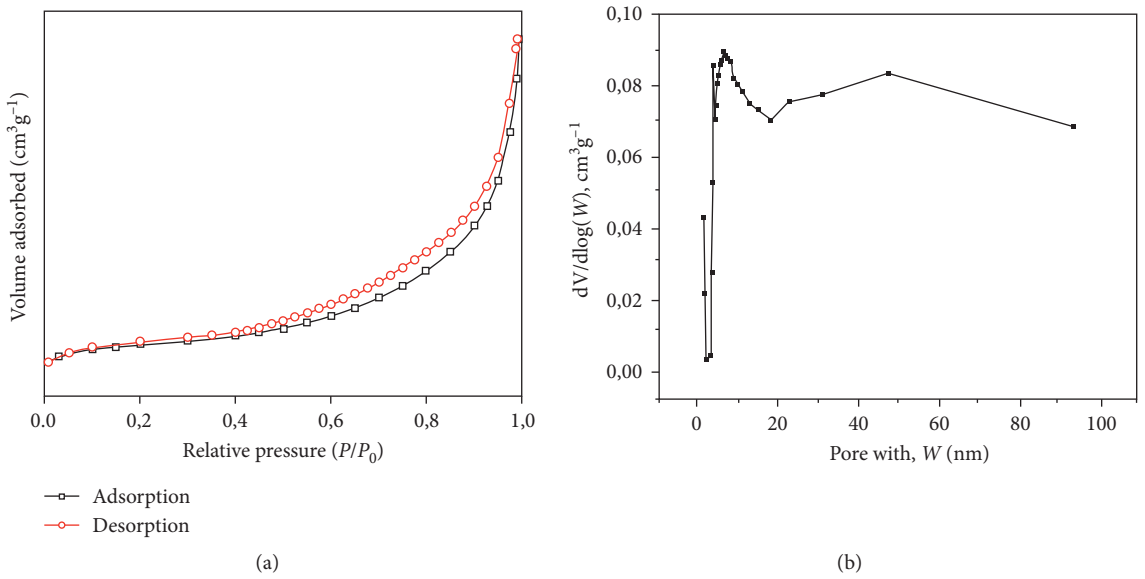

Figure 3: (a) N_2 adsorption-desorption isotherm and (b) BJH pore size distribution of LFO-RHT.

Table 1: Characteristics of LFO-RHT and LFO samples.

Sample	Structural property		
	BET specific surface area (m^2 g^{-1})	Pore volume (cm^3 g^{-1})	Pore size (nm)
LFO-RHT	48.75	0.142	7.87
LFO	8.06	0.028	11.43

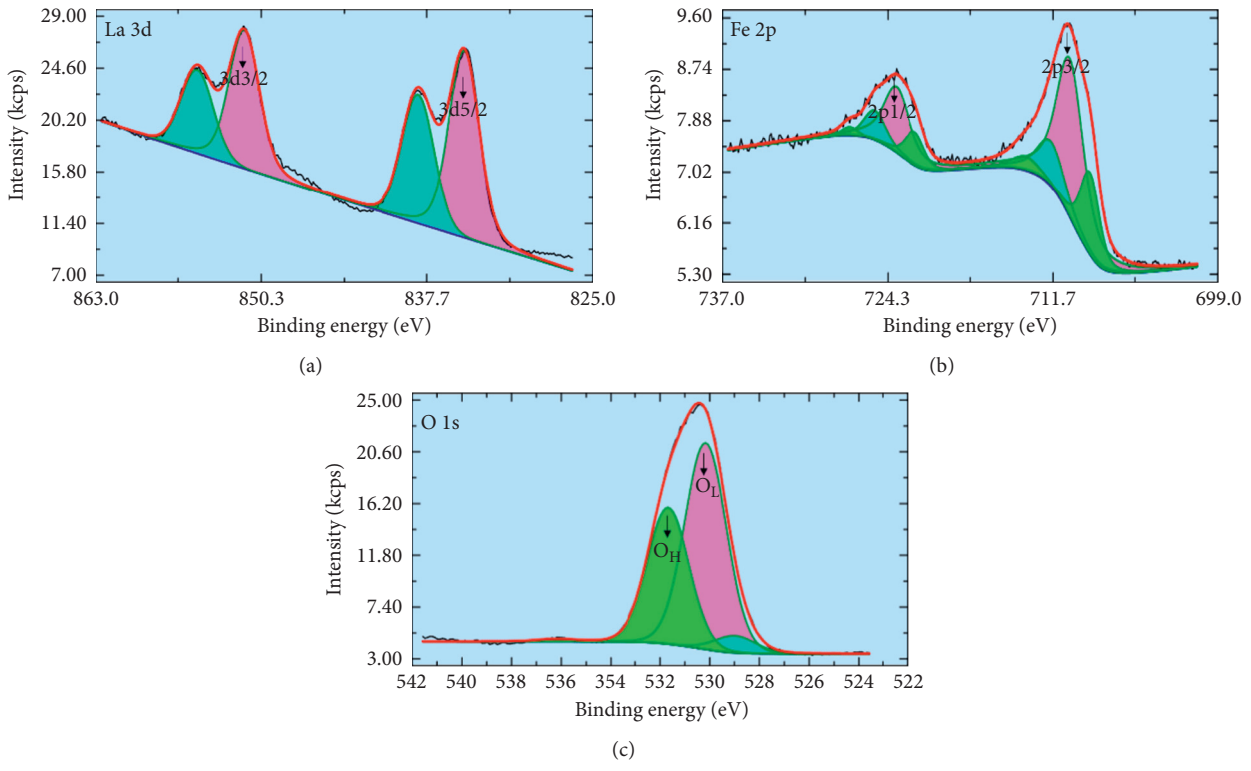

Figure 4: XPS spectra of (a) La 3d, (b) Fe 2p, and (c) O 1s for LFO-RHT.

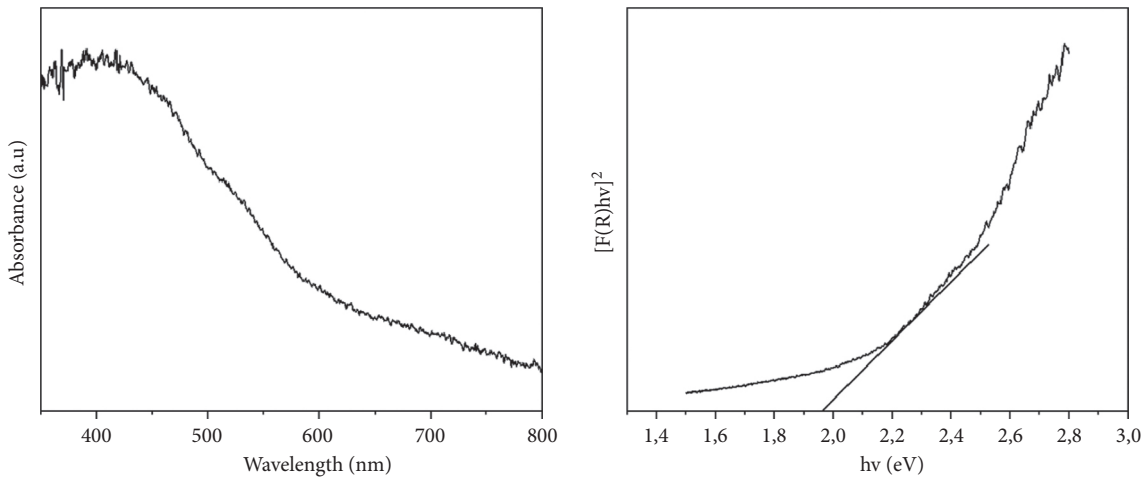

Figure 5: (a) UV-Vis absorption spectra and (b) corresponding [F (R) hυ]2 versus hυ plot.

concentration of 10 mM. However, a decrease of phenol total removal rate by 6.98% was observed when further increasing the concentration of H_2O_2 to 20 mM. The fitting of photo-Fenton catalytic degradation data in Figure 7(b) showed that the reaction rate constants k for phenol degradation in 5 mM, 10 mM, 15 mM, and 20 mM H_2O_2 were 0.0091, 0.0192, 0.0130, and 0.0123 min^{-1}, respectively.

Industrial wastewater could be acidic or basic medium due to its discharging from different industrial activities and thus the effect of pH should be studied. The effect of initial solution pH on phenol photo-Fenton degradation is presented in Figure 7(c). The phenol degradation rate via the photo-Fenton process decreased with increasing pH values, which is consistent with the previous reports [44, 47]. It can be observed that the maximum photo-Fenton degradation of phenol of 94.7% was achieved at pH 5.0 while the degradation rate dropped to 90.8% at pH = 8 and 86.7% at pH = 10. The pseudo-first-order reaction rate constant k was found to be the highest (0.0192 min^{-1}) at pH = 5 as compared with 0.0146, 0.0131, and 0.0112 min^{-1} when at pH = 3, 8, and 10, respectively. This could be explained by the changes in the surface charge of LFO-RHT, the dissociation of phenol, and the generation of hydroxyl radicals during the photo-Fenton reaction. As can be seen from Figure S1, the pH of point zero of charge (pH_{pzc}) of LFO-RHT is 6.05 which is determined by using the pH drift method [29]. At pH below the pH_{pzc} (pH = 3 and 5), the surface of the LFO-RHT is positively charged, whilst at pH above the pH_{pzc} (pH = 8 and 10), it is negatively charged. Meanwhile, phenol is in a molecular form at a neutral or weakly alkaline solution and in phenoxide ion $C_6H_5O^-$ structure at high pH values due to its dissociation [47]. Therefore, at low pH values, there is no electrostatic repulsion between the positively charged surface of LFO-RHT and phenol species. Moreover, the generation of hydroxyl radicals was found to be easier in an acidic medium than in a neutral or basic medium [42]. Noting that, as the solution is too acidic (pH = 3), the excess H^+ ions could react with hydroxyl radicals OH in the solution, leading to a deterioration in the degradation rate [17]. Thus, the highest degradation rate was observed at pH = 5. At pH = 8 and 10, the negatively charged surfaces of LFO-RHT might hinder the adsorption of anion phenoxide species due to the repulsive force, causing a slight decrease in the phenol degradation rate. Jiang and coworkers have reported a similar observation [48]. From a practical application point of view, the degradation of phenol at pH = 5 would be an environmentally friendly process because the pH of the phenol-containing industrial effluents is around 5.

Based on the above results, a possible photo-Fenton catalytic mechanism using LFO-RHT was proposed, as follows:

$$\equiv Fe^{III} + H_2O_2 \longrightarrow Fe^{III}H_2O_2 \quad (6)$$

$$\equiv Fe^{III} + H_2O_2 \longrightarrow Fe^{II} + HO_2 + H^+ \quad (7)$$

$$\equiv Fe^{III} + HO_2 + H^+ \longrightarrow Fe^{II} + O_2 + 2H^+ \quad (8)$$

$$\equiv Fe^{II} + H_2O_2 \longrightarrow Fe^{III} + OH + OH^- \quad (9)$$

$$LFO - RHT + hv \longrightarrow LFO - RHT\left(e^- + h^+\right) \quad (10)$$

$$H_2O_2 + e^- \longrightarrow OH + OH^- \quad (11)$$

$$OH + \text{phenol} \longrightarrow \text{degradation products} \quad (12)$$

As is well known during Fenton-like reaction, the interfacial Fe atoms (denoted as $\equiv Fe^{III}$) of LFO-RHT photocatalyst can react with H_2O_2 to generate OH radicals (equations (6)–(9)) which can directly oxidize phenol to degradation products (equation (12)) [22]. Under visible light irradiation, the LFO-RHT photocatalyst undergoes charge separation which produces electrons (e^-) and holes ($\underline{h}^+$) simultaneously (equation 10). Then, the electron is trapped by H_2O_2 to form the OH as well (equation (11)) [17]. Therefore, the considerable improvement in the rate of phenol removal benefits from the synergism of photocatalysis and heterogeneous Fenton-like reaction.

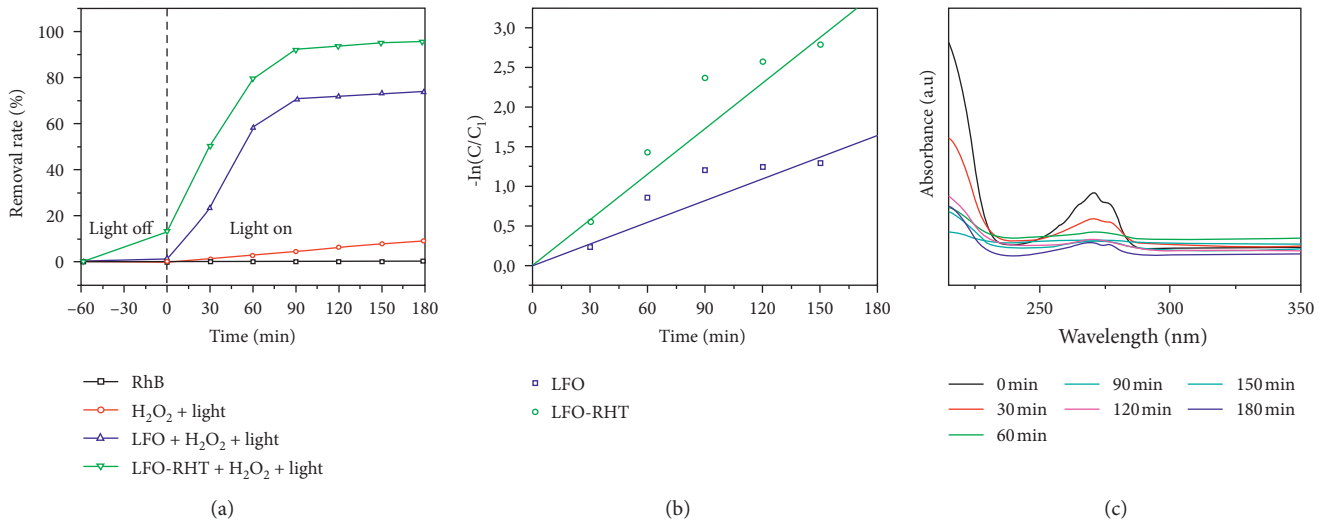

Figure 6: (a) Removal of phenol by adsorption and photo-Fenton reaction using LFO and LFO-RHT catalysts; (b) plots of –ln ($C/C1$) versus irradiation time; and (c) temporal UV-Vis spectral change of phenol aqueous solution versus irradiation time in the photo-Fenton reaction (test conditions: temperature = 25°C; phenol concentration = 20 mg L^{-1}; catalyst dosage = 1 g L^{-1}; H_2O_2 concentration = 10 mM; pH = 5).

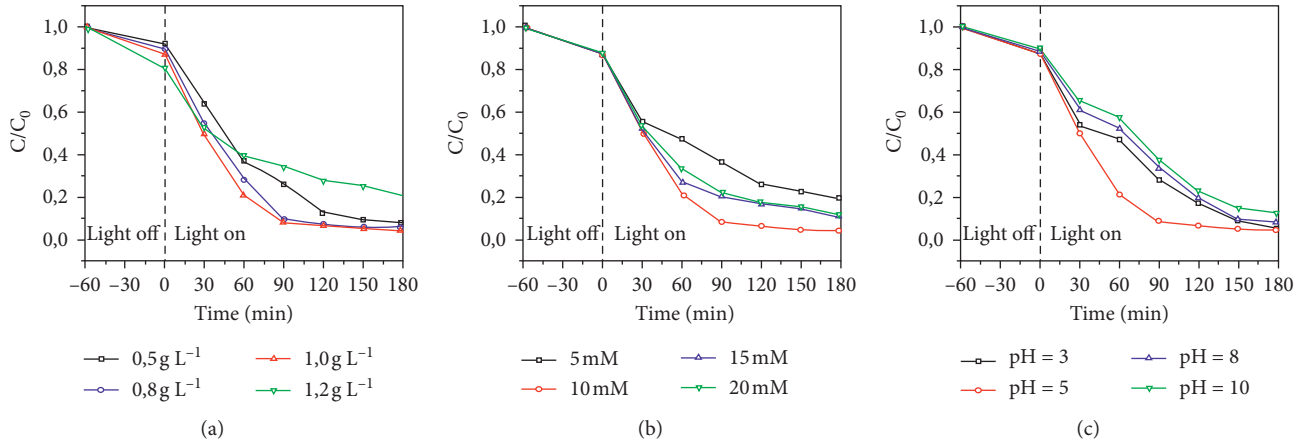

Figure 7: (a) Effect of catalyst dosage (H_2O_2 concentration = 10 mM); (b) H_2O_2 concentration; and (c) initial solution pH (H_2O_2 concentration = 10 mM) on photo-Fenton degradation of phenol (reaction conditions (if not specified): temperature = 25°C, catalyst dosage = 1 g L^{-1}, initial phenol concentration = 20 mg L^{-1}, and initial solution pH = 5).

3.3. Reusability of LFO-RHT Catalyst. Photocatalytic stability is considered as one of the important criteria in evaluating photocatalyst performances. In order to explore the reusability of the as-synthesized catalyst, the stability of the LFO-RHT photocatalyst was evaluated by successive experiments, as shown in Figure 8(a). Obviously, LFO-RHT showed good stability for the photo-Fenton degradation of phenol under visible light irradiation and has no significant loss of activity after 4 recycles. At the fourth experiment, the photo-Fenton degradation rate of phenol is up to 93.47% after 180 min exposure to visible light irradiation, which is relatively similar to the first run (94.7%). Moreover, a comparison of XRD diffraction patterns of the fresh and after 4 recycles of LFO-RHT was performed as shown in Figure 8(b). It was found that there are no significant changes between these two samples, suggesting the stability of LFO-RHT during reaction, which indicates that the LFO-RHT is a stable and reusable photocatalyst in wastewater treatment.

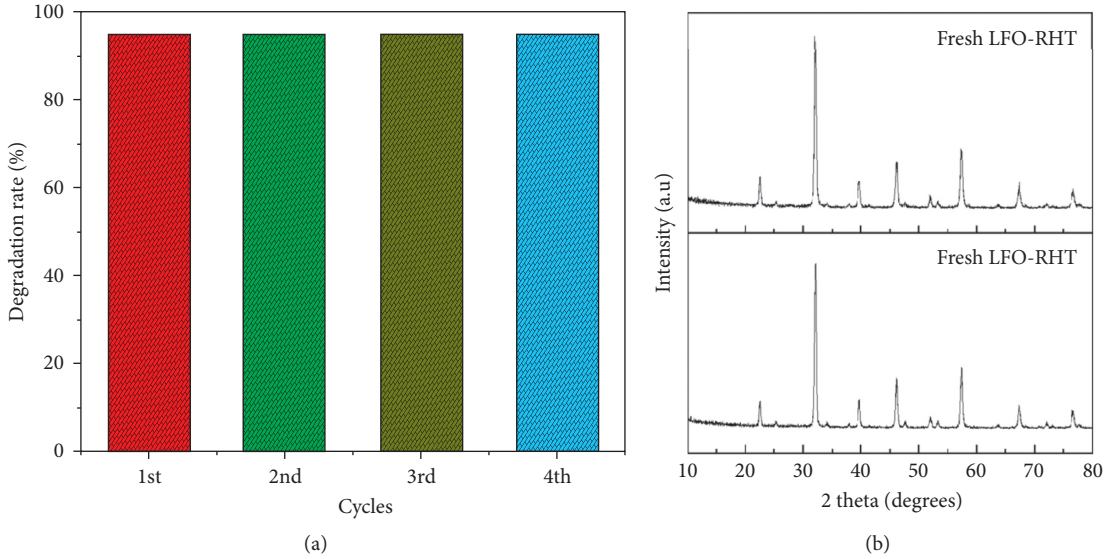

Figure 8: (a) The regeneration and reusability of LFO-RHT for the photo-Fenton degradation of phenol over 4 cycles and (b) XRD patterns of LFO-RHT before and after 4 cycles of photo-Fenton degradation test.

4. Conclusions

Mesoporous $LaFeO_3$ particles with pure perovskite phase have been synthesized via a nanocasting process. Characterization and experimental results showed that $LaFeO_3$ with porous structure could improve the phenol adsorption ability of the photocatalyst and in turn enhance its photo-Fenton catalytic activity, implying synergistic effects of adsorption, and the photo-Fenton process is a good technique for phenol removal. Effects of catalyst dosage, H_2O_2 concentration, and initial solution pH on the photo-Fenton degradation of phenol were systematically investigated. Furthermore, our results proved that mesoporous $LaFeO_3$ exhibited good photo-Fenton catalytic activity and stability even after four cycles and proposed its photo-Fenton catalytic mechanism for the degradation of phenol under visible light.

Data Availability

The data used to support the findings of this study are available from the corresponding author upon request.

Conflicts of Interest

There are no conflicts of interest to declare.

Acknowledgments

This research was funded by the Hanoi University of Science and Technology (HUST) under Project no. T2020-SAHEP-029.

Supplementary Materials

Figure S1: the pH of point of zero charge of LFO-RHT. (*Supplementary Materials*)

References

[1] B. Diya'uddeen, S. R. Pouran, A. R. A. Aziz, S. M. Nashwan, W. M. A. W. Daud, and M. G. Shaaban, "Hybrid of Fenton and sequencing batch reactor for petroleum refinery wastewater treatment," *Journal of Industrial and Engineering Chemistry*, vol. 25, pp. 186–191, 2015.

[2] F. Adam, J. Andas, and I. A. Rahman, "A study on the oxidation of phenol by heterogeneous iron silica catalyst," *Chemical Engineering Journal*, vol. 165, no. 2, pp. 658–667, 2010.

[3] G. M. Salcedo, L. Kupski, J. L. de Oliveira Arias, S. C. Barbosa, and E. G. Primel, "Bojuru sand as a novel catalyst for refinery wastewater treatment and phenol degradation by heterogeneous photo catalysis," *Journal of Photochemistry and Photobiology A: Chemistry*, vol. 402, Article ID 112796, 2020.

[4] X. Zhang, J. Chen, S. Jiang et al., "Enhanced photocatalytic degradation of gaseous toluene and liquidus tetracycline by anatase/rutile titanium dioxide with heterophase junction derived from materials of Institut Lavoisier-125(Ti): degradation pathway and mechanism studies," *Journal of Colloid and Interface Science*, vol. 588, pp. 122–137, 2021.

[5] Y. Wang, R. Wang, N. Lin, Y. Wang, and X. Zhang, "Highly efficient microwave-assisted Fenton degradation bisphenol A using iron oxide modified double perovskite intercalated montmorillonite composite nanomaterial as catalyst," *Journal of Colloid and Interface Science*, vol. 594, pp. 446–459, 2021.

[6] Y. Wang, N. Lin, Y. Gong, R. Wang, and X. Zhang, "Cu-Fe embedded cross-linked 3D hydrogel for enhanced reductive removal of Cr(VI): characterization, performance, and mechanisms," *Chemosphere*, vol. 280, Article ID 130663, 2021.

[7] Y. Wang, R. Wang, L. Yu, Y. Wang, C. Zhang, and X. Zhang, "Efficient reactivity of LaCu0.5Co0.5O3 perovskite intercalated montmorillonite and g-C3N4 nanocomposites in microwave-induced H2O2 catalytic degradation of bisphenol A," *Chemical Engineering Journal*, vol. 401, Article ID 126057, 2020.

[8] L. Hu, P. Wang, G. Zhang et al., "Enhanced persulfate oxidation of organic pollutants and removal of total organic

carbons using natural magnetite and microwave irradiation," *Chemical Engineering Journal*, vol. 383, Article ID 123140, 2020.

[9] O. B. Ayodele, J. K. Lim, and B. H. Hameed, "Degradation of phenol in photo-Fenton process by phosphoric acid modified kaolin supported ferric-oxalate catalyst: optimization and kinetic modeling," *Chemical Engineering Journal*, vol. 197, pp. 181–192, 2012.

[10] L. Di, H. Yang, T. Xian, X. Liu, and X. Chen, "Photocatalytic and photo-Fenton catalytic degradation activities of Z-scheme Ag2S/BiFeO3 heterojunction composites under visible-light irradiation," *Nanomaterials*, vol. 9, no. 3, p. 399, 2019.

[11] V. Kavitha and K. Palanivelu, "The role of ferrous ion in Fenton and photo-Fenton processes for the degradation of phenol," *Chemosphere*, vol. 55, no. 9, pp. 1235–1243, 2004.

[12] M. Antonopoulou, E. Evgenidou, D. Lambropoulou, and I. Konstantinou, "A review on advanced oxidation processes for the removal of taste and odor compounds from aqueous media," *Water Research*, vol. 53, pp. 215–234, 2014.

[13] Y. Yang, W. Ji, X. Li et al., "Insights into the degradation mechanism of perfluorooctanoic acid under visible-light irradiation through fabricating flower-shaped Bi5O7I/ZnO n-n heterojunction microspheres," *Chemical Engineering Journal*, vol. 420, Article ID 129934, 2021.

[14] Y. Yang, Z. Zheng, M. Yang et al., "In-situ fabrication of a spherical-shaped Zn-Al hydrotalcite with BiOCl and study on its enhanced photocatalytic mechanism for perfluorooctanoic acid removal performed with a response surface methodology," *Journal of Hazardous Materials*, vol. 399, Article ID 123070, 2020.

[15] A. Babuponnusami and K. Muthukumar, "Degradation of Phenol in Aqueous Solution by Fenton, Sono-Fenton and Sono-photo-Fenton Methods degradation of phenol in aqueous solution by fenton, sono-fenton and sono-photo-fenton methods," *CLEAN - Soil, Air, Water*, vol. 39, no. 2, pp. 142–147, 2011.

[16] F. Chen, W. An, L. Liu, Y. Liang, and W. Cui, "Highly efficient removal of bisphenol A by a three-dimensional graphene hydrogel-AgBr@rGO exhibiting adsorption/photocatalysis synergy," *Applied Catalysis B: Environmental*, vol. 217, pp. 65–80, 2017.

[17] T. Huang, J. Zhu, S. Ge, T. Guo, C. Jiang, and L. Xie, "Synthesis of novel CdSe QDs/BiFeO3 composite catalysts and its application for the photo-Fenton catalytic degradation of phenol," *Journal of Environmental Chemical Engineering*, vol. 8, no. 5, Article ID 104384, 2020.

[18] P. Garcia-Muñoz, F. Fresno, C. Lefevre, D. Robert, and N. Keller, "Highly robust La1-xTixFeO3 dual catalyst with combined photocatalytic and photo-CWPO activity under visible light for 4-chlorophenol removal in water," *Applied Catalysis B: Environmental*, vol. 262, Article ID 118310, 2020.

[19] Q. Feng, J. Zhou, W. Luo, L. Ding, and W. Cai, "Photo-Fenton removal of tetracycline hydrochloride using LaFeO3 as a persulfate activator under visible light," *Ecotoxicology and Environmental Safety*, vol. 198, Article ID 110661, 2020.

[20] B. Palas, G. Ersöz, and S. Atalay, "Photo Fenton-like oxidation of Tartrazine under visible and UV light irradiation in the presence of LaCuO3 perovskite catalyst," *Process Safety and Environmental Protection*, vol. 111, pp. 270–282, 2017.

[21] Y. Jia, C. Wu, D.-H. Kim et al., "Nitrogen doped BiFeO3 with enhanced magnetic properties and photo-Fenton catalytic activity for degradation of bisphenol A under visible light," *Chemical Engineering Journal*, vol. 337, pp. 709–721, 2018.

[22] P. Garcia-Muñoz, F. Fresno, C. Lefevre, D. Robert, and N. Keller, "Synergy effect between photocatalysis and heterogeneous photo-Fenton catalysis on Ti-doped LaFeO3 perovskite for high efficiency light-assisted water treatment," *Catalysis Science & Technology*, vol. 10, no. 5, pp. 1299–1310, 2020.

[23] Y. Ye, H. Yang, H. Zhang, and J. Jiang, "A promising Ag2CrO4/LaFeO3 heterojunction photocatalyst applied to photo-Fenton degradation of RhB," *Environmental Technology*, vol. 41, no. 12, pp. 1486–1503, 2020.

[24] S. Guan, H. Yang, X. Sun, and T. Xian, "Preparation and promising application of novel LaFeO3/BiOBr heterojunction photocatalysts for photocatalytic and photo-Fenton removal of dyes," *Optical Materials*, vol. 100, Article ID 109644, 2020.

[25] S. Guan, R. Li, X. Sun, T. Xian, and H. Yang, "Construction of novel ternary Au/LaFeO3/Cu2O composite photocatalysts for RhB degradation via photo-Fenton catalysis," *Materials Technology*, pp. 1–13, 2020.

[26] A. Alpay, Ö. Tuna, and E. B. Simsek, "Deposition of perovskite-type LaFeO3 particles on spherical commercial polystyrene resin: a new platform for enhanced photo-Fenton-catalyzed degradation and simultaneous wastewater purification," *Environmental Technology & Innovation*, vol. 20, Article ID 101175, 2020.

[27] T. T. N. Phan, A. N. Nikoloski, P. A. Bahri, and D. Li, "Enhanced removal of organic using LaFeO3-integrated modified natural zeolites via heterogeneous visible light photo-Fenton degradation," *Journal of Environmental Management*, vol. 233, pp. 471–480, 2019.

[28] Y. Ji, Y. Xie, L. Zheng, and F. Xu, "Efficient activation of peroxymonosulfate by porous Co-doped LaFeO3 for organic pollutants degradation in water," *Journal of Solid State Chemistry*, vol. 297, Article ID 122077, 2021.

[29] Y. Wang, J. Ren, Y. Wang et al., "Nanocasted synthesis of mesoporous LaCoO3 perovskite with extremely high surface area and excellent activity in methane combustion," *The Journal of Physical Chemistry C*, vol. 112, no. 39, pp. 15293–15298, 2008.

[30] M. M. Nair, F. Kleitz, and S. Kaliaguine, "Kinetics of methanol oxidation over mesoporous perovskite catalysts," *ChemCatChem*, vol. 4, no. 3, pp. 387–394, 2012.

[31] J. Wang, H. Guo, Y. Liu, W. Li, and B. Yang, "Peroxymonosulfate activation by porous BiFeO3 for the degradation of bisphenol AF: non-radical and radical mechanism," *Applied Surface Science*, vol. 507, Article ID 145097, 2020.

[32] Y. Wang, L. Wang, R. Liu, and X. Li, "Casein templated synthesis of porous perovskite and its application in visible-light photocatalytic degradation of methylene blue," *Materials Science in Semiconductor Processing*, vol. 103, Article ID 104597, 2019.

[33] R. Zhang, P. Li, N. Liu, W. Yue, and B. Chen, "Effect of hard-template residues of the nanocasted mesoporous LaFeO3with extremely high surface areas on catalytic behaviors for methyl chloride oxidation," *Journal of Materials Chemistry A*, vol. 2, no. 41, pp. 17329–17340, 2014.

[34] H. Li, J. Zhu, P. Xiao et al., "On the mechanism of oxidative degradation of rhodamine B over LaFeO3 catalysts supported on silica materials: role of support," *Microporous and Mesoporous Materials*, vol. 221, pp. 159–166, 2016.

[35] D. Zhao, Q. Huo, J. Feng, B. F. Chmelka, and G. D. Stucky, "Nonionic triblock and star diblock copolymer and oligomeric surfactant syntheses of highly ordered, hydrothermally stable, mesoporous silica structures," *Journal of the American Chemical Society*, vol. 120, no. 24, pp. 6024–6036, 1998.

[36] M. Kruk, M. Jaroniec, C. H. Ko, and R. Ryoo, "Characterization of the porous structure of SBA-15," *Chemistry of Materials*, vol. 12, no. 7, pp. 1961–1968, 2000.

[37] T. T. N. Phan, A. N. Nikoloski, P. A. Bahri, and D. Li, "Adsorption and photo-Fenton catalytic degradation of organic dyes over crystalline LaFeO3-doped porous silica," *RSC Advances*, vol. 8, no. 63, pp. 36181–36190, 2018.

[38] Y. Wang, l. Yu, R. Wang, Y. Wang, and X. Zhang, "Reactivity of carbon spheres templated Ce/LaCo0.5Cu0.5O3 in the microwave induced H2O2 catalytic degradation of salicylic acid: characterization, kinetic and mechanism studies," *Journal of Colloid and Interface Science*, vol. 574, pp. 74–86, 2020.

[39] Y. Song, S. Xue, G. Wang et al., "Enhanced photocatalytic decomposition of an organic dye under visible light with a stable LaFeO3/AgBr heterostructured photocatalyst," *Journal of Physics and Chemistry of Solids*, vol. 121, pp. 329–338, 2018.

[40] Y. Wang, F. Qin, Z. Yi et al., "Effect of slit width on surface plasmon resonance," *Results in Physics*, vol. 15, Article ID 102711, 2019.

[41] B. M. Pirzada and Pushpendra, B. S. Kunchala, Synthesis of LaFeO3/Ag2CO3 nanocomposites for photocatalytic degradation of Rhodamine B and p-Chlorophenol under natural sunlight," *ACS Omega*, vol. 4, no. 2, pp. 2618–2629, 2019.

[42] T. T. N. Phan, A. N. Nikoloski, P. A. Bahri, and D. Li, "Optimizing photocatalytic performance of hydrothermally synthesized LaFeO3 by tuning material properties and operating conditions," *Journal of Environmental Chemical Engineering*, vol. 6, no. 1, pp. 1209–1218, 2018.

[43] X. Wei, H. Wu, G. He, and Y. Guan, "Efficient degradation of phenol using iron-montmorillonite as a Fenton catalyst: importance of visible light irradiation and intermediates," *Journal of Hazardous Materials*, vol. 321, pp. 408–416, 2017.

[44] L. Yu, J. Chen, Z. Liang, W. Xu, L. Chen, and D. Ye, "Degradation of phenol using Fe3O4-GO nanocomposite as a heterogeneous photo-Fenton catalyst," *Separation and Purification Technology*, vol. 171, pp. 80–87, 2016.

[45] J. Feng, X. Hu, P. L. Yue, H. Y. Zhu, and G. Q. Lu, "Degradation of azo-dye orange II by a photoassisted Fenton reaction using a novel composite of iron oxide and silicate nanoparticles as a catalyst," *Industrial and Engineering Chemistry Research*, vol. 42, no. 10, pp. 2058–2066, 2003.

[46] H. Kusic, N. Koprivanac, A. Bozic, and I. Selanec, "Photo-assisted Fenton type processes for the degradation of phenol: a kinetic study," *Journal of Hazardous Materials*, vol. 136, no. 3, pp. 632–644, 2006.

[47] M. Khraisheh, L. Wu, A. a. H. Al-Muhtaseb, A. B. Albadarin, and G. M. Walker, "Phenol degradation by powdered metal ion modified titanium dioxide photocatalysts," *Chemical Engineering Journal*, vol. 213, pp. 125–134, 2012.

[48] Z. Jiang, L. Wang, J. Lei, Y. Liu, and J. Zhang, "Photo-Fenton degradation of phenol by CdS/rGO/Fe2+ at natural pH with in situ-generated H2O2," *Applied Catalysis B: Environmental*, vol. 241, pp. 367–374, 2019.